JVSTA Journal of Vacuum Science & Technology A

# Electronic structure and stability of II–VI semiconductors and their alloys: The role of metal d bands

S.-H. Wei and Alex Zunger

Citation: Journal of Vacuum Science & Technology A **6**, 2597 (1988); doi: 10.1116/1.575515
View online: http://dx.doi.org/10.1116/1.575515
View Table of Contents: http://scitation.aip.org/content/avs/journal/jvsta/6/4?ver=pdfcov
Published by the AVS: Science & Technology of Materials, Interfaces, and Processing

# Electronic structure and stability of II–VI semiconductors and their alloys: The role of metal *d* bands

S.-H. Wei and Alex Zunger
*Solar Energy Research Institute, Golden, Colorado 80401*

(Received 22 December 1987; accepted 17 February 1988)

It has been traditionally accepted in various theoretical approaches to II–VI semiconductors (e.g., tight binding, pseudopotentials) to neglect the effects of the cation *d* bands, hoping that in some sense they are "deep," "localized," and hence, unresponsive to many perturbations of chemical interest. There are, however, two qualitative reasons to think that this is not so: first, *d* bands in II–VI's are only 7–11 eV below the valence-band maximum (VBM) (i.e., *inside* the main valence band), and second, in tetrahedral (but not octahedral) symmetry, cation *d* orbitals have the same representation ($\Gamma_{15}$) as the anion *p* orbitals, hence the two can interact. We have considered the effects of the cation *d* bands in II–VI's on both the electronic and structural properties of the binary and ternary compounds, treating all electrons on the same footing, in a self-consistent first-principles manner. We find that the *d* orbitals: (i) reverse the *direction* of charge transfer in the alloy (e.g., relative to *s–p* tight binding), (ii) reverse the trends in the spin–orbit splitting at the VBM in the series ZnTe→CdTe→HgTe, (iii) are responsible for most of the valence-band offset between, e.g., HgTe–CdTe, (iv) affect the structural stability, equilibrium lattice parameters, and bulk moduli. We also discuss the equilibrium bond lengths, formation enthalpies, and degree of clustering of inter-II–VI systems $A_n^{II}B_{4-n}^{II}Te_4$ comparing the results to experiment and to simpler tight-binding models.

## I. INTRODUCTION

The electronic structure of II–VI semiconductors $ZnX^{VI}$, $CdX^{VI}$, and $HgX^{VI}$ is distinguished from that of both column IIA chalcogenides $CaX^{VI}$, $SrX^{VI}$, and $BaX^{VI}$ and from the III–V semiconductors by having a cation *d* band *inside* the main valence band. These valence *d* bands are evident in photoemission spectra[1–3] (Fig. 1 and Table I) and in all-electron band-structure calculations[4–11] (Fig. 2), both exhibiting a moderately narrow ($\lesssim 1$ eV), fully occupied metal *d* band around 7–11 eV below the valence band maximum, or 6–2 eV *above* its minimum. In early electronic structure calculations for II–VI semiconductors, the metal *d* bands were retained (see also more recent results in Refs. 7–11). However, most current calculations, using empirical,[12–18] semiempirical,[19] or first-principles[20,21] pseudopotential approaches, as well as tight-binding approaches[22–24] to bulk II–VI semiconductors, their alloys[25–29] and their impurity states[30–32] have ignored the metal *d* bands, assuming them to be a part of the chemically inert atomic cores. The underlying thought in these approaches seems to have been that the *d* bands in II–VI semiconductors are nonbonding, energetically removed from the outer valence orbitals and difficult to treat explicitly in either pseudopotential or tight-binding methods and hence are best explicitly discarded from the spectrum and represented only implicitly through their indirect effects on the valence *s* and *p* electrons.

Indeed the *indirect* effects of *d* orbitals on the properties of IIB–VI semiconductors can be taken into account by models that explicitly neglect[12–32] the *d bands*, by using sufficiently tightly bound (relative to group-IIA atoms) metal *s* orbital energies or sufficiently attractive metal pseudopotentials. It is then possible to fit, for example, the calculated low-lying band gaps of such compounds to experiment. Manipulating atomic quantities (atomic orbital energies and pseudopotentials) could, however, misrepresent the *direct* effects of the *d* orbitals in the solid-state phase, i.e., the *p–d hybridization effects* which can change the band gaps, charge distribution, and the equilibrium structural properties.

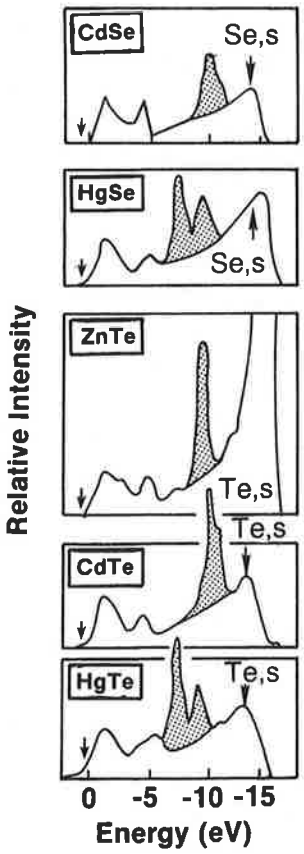


FIG. 1. Observed photoemission spectra (Refs. 1–3) of cation *d* states (shaded regions) in the II–VI compounds. The arrow at $E = 0$ points to the valence-band maximum.

 0734-2101/88/042597-15$01.00  

TABLE I. Experimentally observed cation $d$ band binding energies (in eV) with respect to valence-band maximum. When two values are given for a compound, the first corresponds to $J = 5/2$ and the second to $J = 3/2$ spin–orbit components.

| | Reference 1 | Reference 2 | Reference 3 |
|---|---|---|---|
| ZnO,3$d$ | ··· | 8.81 | 8.5 |
| ZnS,3$d$ | ··· | 9.03 | ··· |
| ZnSe,3$d$ | ··· | 9.20 | 8.9 |
| ZnTe,3$d$ | 9.5 | 9.84 | 9.1 |
| | 9.8 | | |
| CdS,4$d$ | ··· | 9.64 | 10.0 |
| CdSe,4$d$ | 9.55 | 10.04 | 10.7 |
| | 10.28 | | |
| CdTe,4$d$ | 10.09 | 10.49 | 10.5 |
| | 10.72 | | |
| HgSe,5$d$ | 7.33 | ··· | ··· |
| | 9.13 | | |
| HgTe,5$d$ | 7.70 | 7.87 | 7.6 |
| | 9.55 | 9.64 | 9.5 |

In this paper we study the extent to which the metal $d$ orbitals in II–VI semiconductors can be viewed as corelike, chemically inert states. We use all-electron band-structure and total energy techniques which treat the outer metal $d$ electrons on the same footing as other valence electrons. We compare the results with those in which the $d$ bands are omitted or frozen. We establish the effects of these metal $d$ bands on: (i) band gaps; (ii) spin–orbit splittings at the valence-band maximum; (iii) ground-state properties such as equilibrium lattice parameters, cohesive energies, formation enthalpies, and bulk moduli; and (iv) valence-band offsets between semiconductors. Significant $d$-electron effects are found in all of the above quantities.

## II. $p$–$d$ COUPLING IN TETRAHEDRAL STRUCTURE: ESSENTIAL PHYSICS

Whereas the octahedral space group ($O_h^5$) akin to the NaCl structure has inversion symmetry, the tetrahedral space group ($T_d^2$) pertinent to zinc-blende compounds does not. Consequently, symmetry representations of $O_h^5$ do not mix even and odd angular momenta (e.g., $p$ with $d$), whereas those of $T_d^2$ do.[33] This has some obvious implications on the band structure of tetrahedrally bonded compounds near the band-gap region.

Consider, for example, a zinc-blende crystal and ignore for a moment the cation $d$ states. The states near the Fermi energy can be described qualitatively by a simple tight-binding model retaining the cation $p$ orbitals ($p^c$ with energy $\epsilon_p^c$) and the anion $p$ orbitals ($p^a$, with energy $\epsilon_p^a$). Since both have the same symmetry representation $\Gamma_{15}$ (also termed $t_2$), they can interact [Fig. 3(a)] through a coupling matrix element $V_{pp}$. They hence form a lower energy bonding state at the energy

$$\epsilon[\Gamma_{15v}(p)] = \frac{\epsilon_p^c + \epsilon_p^a}{2} - \left[\frac{(\epsilon_p^a - \epsilon_p^c)^2}{4} + V_{pp}^2\right]^{1/2} \quad (1)$$

and an antibonding state at

$$\epsilon[\Gamma_{15c}(p)] = \frac{\epsilon_p^c + \epsilon_p^a}{2} + \left[\frac{(\epsilon_p^a - \epsilon_p^c)^2}{4} + V_{pp}^2\right]^{1/2}. \quad (2)$$

The bonding state has no node and its energy is lowered relative to $\epsilon_p^a$ [Fig. 3(a)].

If, however, cation $d$ states are included at an energy $\epsilon_d^c$ [Fig. 3(b)], they too have a representation of $t_2$ symmetry (their $\Gamma_{12}$, or $e$-symmetry state cannot couple to $l = 1$, hence it remains unshifted) and can couple, through a matrix element $V_{pd}$ to the $p$-like anion state. One can estimate semiquantitatively the magnitude of these $p$–$d$ couplings by considering the $p$–$d$ repulsion energy perturbatively, as

$$\Delta E_{pd} \simeq V_{pd}^2/(\epsilon_p^a - \epsilon_d^c). \quad (3)$$

The magnitude of the energy denominator can be approximated by difference of atomic orbital energies, e.g., using semirelativistic local density orbital energies. Estimating $V_{pd}$ from Harrison's[22(a)] formula $V_{pd} = A(r_d^{3/2}/d^{7/2})$, where $r_d$ and $d$ are the cation $d$-orbital radius and the average bond length, respectively, one finds $V_{pd} \simeq 1$–$2$ eV. This suggests that the $p$–$d$ repulsion shifts the valence-band maximum to higher energies by $\Delta E_{pd}$, of the order of 0.1 to 0.2 eV

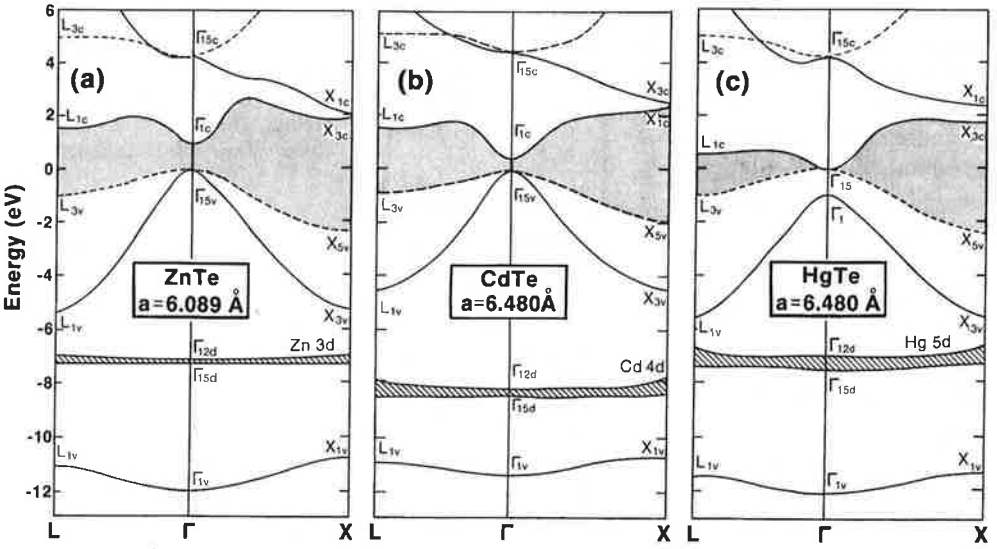


FIG. 2. Calculated (LAPW) band structure of (a) ZnTe, (b) CdTe, and (c) HgTe near their equilibrium lattice constants. The cation $d$ bands are highlighted by the dashed lines. The band-gap regions are shaded. Dashed lines indicate doubly degenerate states.

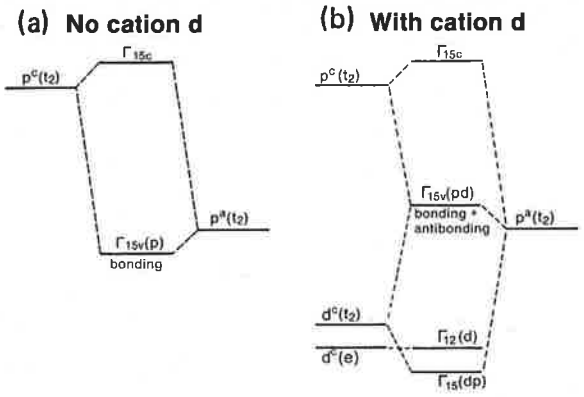


FIG. 3. Schematic plot of *pp* and *pd* coupling in zinc-blende semiconductor: (a) *pp* coupling only and (b) inclusion of *pp* and *pd* coupling.

for III–V compounds, but of order 1 eV for II–VI compounds. It thus appears from these simple estimates that *p–d* repulsion cannot be neglected in II–VI semiconductors. Quantitative calculations, supporting this simple expectation (using all-electron first-principles methods) will be presented in Sec. IV.

This qualitative model (Fig. 3) points to the main consequences of *p–d* repulsion in II–VI semiconductors:

(i) It reduces the direct band gap by repelling $\Gamma_{15v}$ upwards without affecting the direct conduction-band minimum (of $\Gamma_{1c}$ symmetry, hence non-*pd*). A particularly striking example is provided by the fact that despite the greater ionicity of ZnO, it has a *smaller* band gap ($\sim 3.4$ eV[34] in its wurtzite form) than ZnS (3.90 and 3.82 eV for wurtzite and zinc-blende forms, respectively[35]). This is contrary to the situation encountered in salts which lack active *d* bands, e.g., CaO, SrO, and BaO have *larger* band gaps (7.1, 5.3, and 4.4 eV, respectively[34]) then the corresponding less ionic sulfides CaS, SrS, and BaS (5.8, 4.8, and 3.9 eV, respectively[34]). We suggest that the reason for this is the stronger *p–d* repulsion in ZnO (where the Zn 3*d* to O 2*p* orbital energy difference is small) relative to ZnS (having a larger Zn 3*d* to *S* 3*p* orital energy difference). Again, empirical adjustment of the band-structure parameters can be used to reproduce the experimental band gap even if the *d* bands are ignored.[15(c)] However, the physical mechanism leading to these trends remains obscure in such approaches.

(ii) Since *p–d* repulsion raises the energy of the valence-band maximum $E_v$ in inverse proportion to the anion $p$ — cation $d$ energy difference [Eq. (3)], common-anion materials AC and BC whose cations A and B have different *d* orbital energies would also have different values of $\Delta E_{pd}$. The difference $\delta_{pd} = \Delta E_{pd}(\mathrm{AC}) - \Delta E_{pd}(\mathrm{BC})$ will hence contribute to the valence-band discontinuity between the semiconductors AC and BC (Sec. IV E).

(iii) *p–d* coupling admixes *d* character into the wave function at the valence-band maximum. (This is verified by direct calculations, see Sec. IV B.) Since *d* states contribute oppositely to the spin–orbit splitting (lowering it), relative to *p* orbitals (which raise it), *p–d* coupling would hence affect the trends in spin–orbit energies. This will be discussed in Sec. IV C.

(iv) Whereas classical point-ion crystal-field models[33] predict for $T_d$ symmetry that the *e* level is below the $t_2$ level, *p–d* repulsion, neglected by crystal field models can reverse the level ordering. This is the case for II–VI compounds (see Fig. 2) where band-structure calculations indeed find[5–10] that the $\Gamma_{15}$ ($pd$) band ($t_2$-like) is *below* the $\Gamma_{12}$ ($d$) ($e$-like) band.

(v) Two-level perturbation theory for *nonoverlapping* orbitals would suggest that *p–d* repulsion does not change the cohesive energy (since this repulsion displaces the bonding $\Gamma_{15}$ ($d$) and antibonding $\Gamma_{15}$ ($p$) by equal amounts to opposite directions, but *both* of these states are occupied). However, since *p–d* orbitals overlap in crystal, their mutual repulsion also modifies the $\Gamma_{15}$ wave functions, which in turn could affect the cohesive energy. In particular, the *p–d* repulsion diminishes the content of *p* orbitals in the upper valence band and, in raising the energy of the valence-band maximum (VBM), also spreads out its wave function. This is likely to lead to a larger equilibrium volume (lattice parameter) relative to the pure *p* case. This conjecture is supported by our calculation discussed in Sec. IV A.

## III. METHOD OF CALCULATION

We have used the self-consisted first-principles general potential linearized augmented plane-wave (LAPW) method[36] within the local density functional formalism[37] to calculate the properties of ZnTe, CdTe, HgTe, and their ordered ternary compounds. We used the Hedin–Lundqvist exchange and correlation formula.[38] The details of this method can be found elsewhere.[36]

Since we are studying compounds with heavy atom constituents, scalar relativistic effects[39] (i.e., all the relativistic effects except spin–orbit coupling), are included for all valence states (including the outermost cation *d* states). Core states are calculated fully relativistically using an atomiclike approach (i.e., retaining only the spherical part of the potential). No shape approximations are made to the crystal potential and charge density. All states (including the core states) are calculated fully self-consistently.

## IV. RESULTS

### A. Ground-state properties of binary and ternary II–VI's

To qualitatively assess the effect of *p–d* repulsion on the ground-state properties, we compare in Table II[40–46] the results obtained here (retaining the cation *d* bands) with those obtained using the first-principles pseudopotential method[20] [assuming frozen $(n-1)d$ cation orbitals, hence, no cation *d* band in the valence band]. The latter method incorporates the *indirect* effects of the *d* orbitals on the atomic valence *s* and *p* pseudopotentials but lacks *d*-band *wave functions* in the solid, hence misses entirely the symmetry induced *p–d* repulsion effect. Comparison of the calculated ground-state properties with experiment (Table II) shows a rather good agreement when the cation *d* bands are retained (present results). Note, however, that the underlying local density

formalism itself is not free of error; for example, we find $a_{eq}$ of HgTe to be larger than $a_{eq}$ of CdTe by 0.022 Å, whereas the experimental results[41,42] show $a_{eq}$(HgTe) to be smaller than $a_{eq}$(CdTe) by 0.02 Å. Similarly, our calculated cohesive energies are too large by 1–1.5 eV, mainly a consequence of neglecting multiplet stabilization energies (more negative in the free atoms than in the solids and decreasing along the Zn→Cd→Hg sequence).[47] However, the discrepancies relative to experiment evident in the "no $d$" pseudopotential calculation far exceed the error limits of the local density method or the intrinsic convergence errors. When the cation $d$ bands are omitted (pseudopotential results,[20] denoted in Table II as no $d$), the predicted lattice constants are too small relative to experiment by 7.7%, 10.2%, and 13%; and the predicted bulk moduli are too small by 46%, 70%, and 90% for ZnTe, CdTe, and HgTe, respectively. These errors are particularly large for HgTe which has the shallowest (and most spatially delocalized) cation $d$ orbitals, hence, the strongest $p$–$d$ repulsion. Whereas such systematic discrepancies can be fixed by adding an empirical repulsive potential adjusted to match the experimental ground-state properties,[20] the need for such substantial adjustments (for II–VI's, but not for III–V's) testifies to the significant role of $p$–$d$ repulsions in these systems. It would also suggest that $p$–$d$ repulsion, in depleting $p$ character from the upper valence band and delocalizing its wave function, leads to a larger equilibrium lattice constant relative to the pure $p$ case.

Calculations of alloy phase diagrams (see Sec. IV F) often require the knowledge of the relative cohesive energies $\Delta H$ of an ordered *ternary* phase[48] (e.g., $CdHgTe_2$) with respect to equivalent amounts of the binary constituents (e.g., CdTe + HgTe). It is interesting to note that calculation techniques which omit $p$–$d$ repulsion have produced overly negative formation enthalpies, e.g., $\Delta H = -0.6$ meV/4-atoms using tight binding,[49] or $\Delta H = -60$ meV/4-atoms using pseudopotentials[20] for $CdHgTe_2$ in the CuAuI-like structure, compared with the present result of $\Delta H = +12.3$ meV/4-atoms. Whereas the small magnitude of these energies[49] and the numerical intricacies involved in obtaining them make it difficult to quantitatively assess their precision, our foregoing discussion suggests that here, too, the omission of the destabilizing $p$–$d$ repulsion could be responsible for the predicted stability of the ordered phase[20,49] by both tight-binding and pseudopotential methods, compared with the instability predicted here. (No ordering is found experimentally.)

## B. Antibonding *d* character in the upper valence bands

Figure 2 depicts the calculated band structures of ZnTe, CdTe, and HgTe. Table III[50–58] summarizes some of the band-structure parameters. Inspection of the orbital character of the various band states in ZnTe, CdTe, and HgTe reveals a number of interesting features: (i) states that can mix $d$ character by symmetry, do so. This is evident at the valence-band maximum $\Gamma_{15v}$ (7.2%, 7.4%, and 12.9% cation $d$ character in the cation muffin-tin spheres of ZnTe, CdTe, and HgTe, respectively); in $\Gamma_{15c}$ (10.6%, 9.2%, and 9.7% anion $d$ character in ZnTe, CdTe, and HgTe, respectively) and in $X_{3v}$ (6.5%, 2.8%, and 15.1% cation $d$ character in ZnTe, CdTe, and HgTe, respectively). (ii) States forming the anion $s$ band at the bottom of the valence band (e.g., $X_{1v}$ and $L_{1v}$) are found to include also contributions from the cation $d$ states: 6.4%, 15.8%, and 9.3% in $X_{1v}$, and 4.1%, 11.2%, and 6.4% in $L_{1v}$, for ZnTe, CdTe, and HgTe, respectively. This suggests that the photoemission peak normally associated with the anion $s$ band (indicated in Fig. 1 by an arrow near $\sim -12$ eV) could exhibit a contribution (e.g., a low-energy shoulder in ZnTe and CdTe) due to the tailing density of states of the *cation d* band. This effect is absent in the photoemission spectra of III–V compounds lacking a $d$ band (e.g., BP, AlP). Furthermore, since the $L_{1v}$ and $X_{1v}$ states contain $d$ character, but the $\Gamma_{1v}$ does not (by symmetry), $p$–$d$ repulsion acts to *narrow* the lowest, $L_{1v}$–$\Gamma_{1v}$–$X_{1v}$

TABLE II. Comparison of calculated ground-state properties of II–VI compounds (lattice parameter $a$, cohesive energy $E_c$, and bulk modulus $B$) using the present all-electron (LAPW) approach which retains the cation $d$ band, and a pseudopotential (ps) approach which does not. Both calculations are semirelativistic. Experimental results are given for comparison.

| | ZnTe | | | CdTe | | | HgTe | | |
|---|---|---|---|---|---|---|---|---|---|
| Property | With $d$ (LAPW)[a] | Exptl. | No $d$ (ps)[b] | With $d$ (LAPW)[a] | Exptl. | No $d$ (ps)[b] | With $d$ (LAPW)[a] | Exptl. | No $d$ (ps)[b] |
| $a$ (Å) | 6.052 | 6.089[c] | 5.618 | 6.470 | 6.481[d] | 5.818 | 6.492 | 6.461[e] | 5.616 |
| $E_c$ (eV/pair) | 5.64 | 4.82[f] | 6.75 | 5.35 | 4.45[f] | 6.77 | 4.46 | 3.22[f] | 7.05 |
| $B$ (GPa) | 52.1 | 50.9[g] | 27.3 | 44.0 | 44.5[h] | 13.3 | 46.1 | 47.6[h] | 4.7 |

[a] Present results.
[b] Pseudopotential study of Ref. 20 in which the cation $d$ band is frozen. This calculation, like the one reported here, uses the Hedin–Lindqvist exchange-correlation functional.
[c] Reference 40.
[d] Reference 41.
[e] Reference 42.
[f] References 43 and 44.
[g] Reference 45.
[h] Reference 46.

TABLE III. Calculated band gaps $E_g$, center of $d$ band energies $\epsilon_d$, spin–orbit splittings of valence bands at $\Gamma(\Delta_0)$, and $L(\Delta_1)$, and that of the cation $d$ bands $\Delta_d$, for ZnTe, CdTe, and HgTe. NR, SR, and R denote nonrelativistic, semirelativistic, and relativistic calculations, respectively. All the energies are in eV.

| | ZnTe | | | CdTe | | | HgTe | | |
|---|---|---|---|---|---|---|---|---|---|
| | LMTO[a] | LAPW[b] | Exptl. | LMTO[a] | LAPW[b] | Exptl. | LMTO[c] | LAPW[b] | Exptl. |
| $E_g$ (NR) | ··· | 1.98 | ··· | ··· | 1.44 | ··· | ··· | 1.14 | ··· |
| $E_g$ (SR) | 0.96 | 1.02 | ··· | 0.51[a] | 0.47 | ··· | ··· | −0.99 | ··· |
| $E_g$ (R) | 0.63 | 0.72 | 2.39[d] | 0.29,[a] 0.47[c] | 0.18 | 1.59[e] | −1.06 | −1.27 | −0.30[f] |
| $\epsilon_d$ | −7.2 | −7.18 | −9.84[g] | −8.55,[a] −7.80[c] | −8.33 | −10.49[g] | −7.38 | −7.18 | −8.58[g] |
| $\Delta_0$ | 1.01 | 0.89 | 0.91[h] | 0.90,[a] 0.95[c] | 0.86 | 0.90[i] | 0.90 | 0.78 | 1.08[j] |
| $\Delta_1$ | 0.58 | 0.51 | 0.53[k] | 0.55,[a] 0.57[c] | 0.53 | 0.54[k] | 1.31[l] | 0.53 | 0.62[k] |
| $-\Delta_d$ | ··· | 0.37 | 0.3[m] | 0.5[c] | 0.69 | 0.63[m] | 1.7 | 1.68 | 1.85[m] |

[a] See Ref. 50 for details.
[b] Present results.
[c] Reference 51.
[d] Reference 52.
[e] Reference 53.
[f] Reference 54.
[g] Reference 2.
[h] Reference 55.
[i] Reference 56.
[j] Reference 57.
[k] Reference 58.
[l] Reference 51; this could be a printing error.
[m] Reference 1.

valence band (while broadening the upper $L_{1v}$–$\Gamma_{15v}$–$X_{3v}$ valence band). (iii) The conduction-band minimum at $\Gamma_{1c}$, described by tight-binding methods[22–26] as a *cation s* state, has significant *anion* character as well, e.g., 28.2%, 24.2%, and 25.5% for ZnTe, CdTe, and HgTe, respectively.

The simple tight-binding argument for *p–d* mixing described in Sec. II and Fig. 3(b) suggests the antibonding character in the valence-band maximum state $\Gamma_{15v}$ to be the hallmark of *p–d* mixing. Figure 4(a) depicts the calculated wave function square for the $\Gamma_{15v}$ state in HgTe, clearly exhibiting a minimum along the Hg–Te bond direction (partially a consequence of the ionicity of this bond) and characteristic *antibonding lobes* around the Hg site (i.e., pointing *away* from the nearest bonded atoms, towards the interstitial sites). These antibonding lobes are absent in the $\Gamma_{15v}$ state of semiconductors which lack any significant *p–d* repulsion (e.g., III–V's). Similar antibonding features are exhibited, e.g., by the $L_{3v}$ state [Fig. 4(b)] and the $X_{5v}$ state [Fig. 4(c)], all absent in the analogous states in III–V compounds. The antibonding character mixed into the valence-band maximum in II–VI compounds reflects the constraint of orthogonality to the corresponding $\Gamma_{15}$ state of the metal *d* band [$\Gamma_{15}(dp)$ in Fig. 3]. This is demonstrated in Fig. 5(a) which depicts the charge density contributed by this $\Gamma_{15}(dp)$ state, showing its *bonding* charge buildup, oriented *along* the Hg–Te bond. (Note that the $\Gamma_{12d}$ state, depicted in Fig. 5(b), is nonbonding and has its atomiclike charge distribution.)

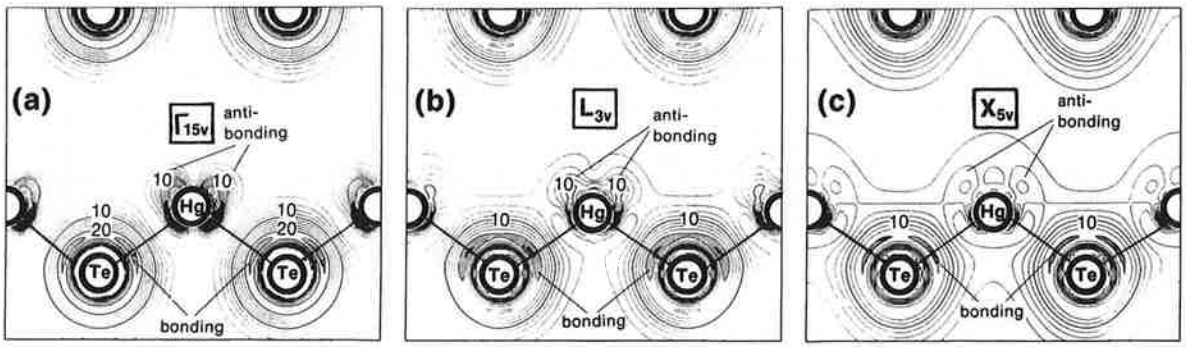


FIG. 4. Calculated wave-function amplitudes of the $\Gamma_{15v}$ (a), $L_{3v}$ (b), and $X_{5v}$ (c) for HgTe.

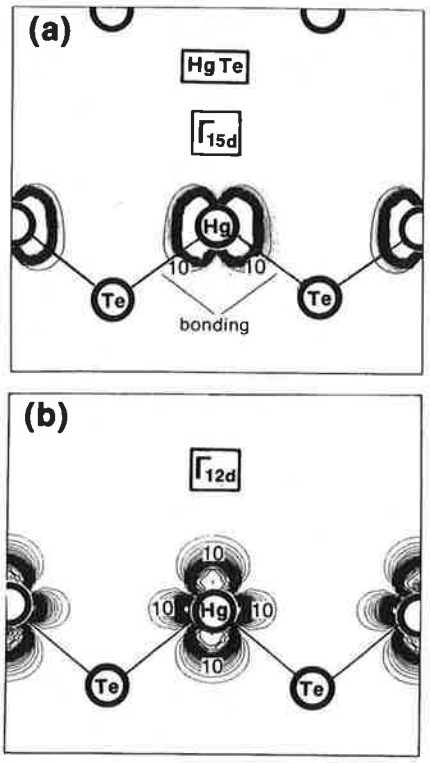


FIG. 5. Wave-function amplitude for $d$ band states in HgTe: (a) $\Gamma_{15d}$ and (b) $\Gamma_{12d}$. Note the bonding buildup of charge along the bond in (a) and the nonbonding character in (b).

To directly isolate the effect of $p$–$d$ repulsion on the ground-state charge density, we have repeated band-structure calculations for CdTe and HgTe where the cation $d$ orbitals are effectively removed from the basis set. This was done by setting the LAPW energy parameters[36] $E^{\mathrm{Cd}}_{l=2}$ and $E^{\mathrm{Hg}}_{l=2}$ for the $d$ wave basis functions inside the Cd and Hg spheres to values which are distant from the corresponding $d$ band energies. We then plot the resulting total valence-band charge densities (from the $\Gamma_{15v}$ to the $\Gamma_{1v}$ state, without the contribution of the cation $d$ states) in Fig. 6(a) (for HgTe) and Fig. 6(b) (for CdTe). Comparison with the valence charge densities of HgTe and CdTe calculated *with* $p$–$d$ repulsions (i.e., retaining the cation $d$ band in the variational calculations) is given in Figs. 6(c) and 6(d), respectively, whereas Figs. 6(e) and 6(f) give the differences in charge densities induced by $p$–$d$ repulsion effects [i.e., (c)–(a) in Fig. 6(e) and (d)–(b) in Fig. 6(f)]. Inspection of these results shows that $p$–$d$ repulsion *depletes* bonding charge from the cation–anion bond (negative contours, depicted in Figs. 6(e) and 6(f) by dashed contours), and deposits it in the antibonding direction around the cation site (lobes pointing *away* from the bond direction). This $p$–$d$ repulsion-induced bond weakening (more pronounced in HgTe, with its shallow and delocalized $d$ electrons) could be the reason that our calculated cohesive energies of these materials are smaller relative to calculations which omit the cation $d$ bands (Table II).

### C. Spin–orbit splittings

Spin–orbit (SO) splittings exhibit opposite contributions from $p$ and $d$ orbitals,[59,60] hence constitute an interesting measure to the $p$–$d$ hybridization discussed in the previous section.

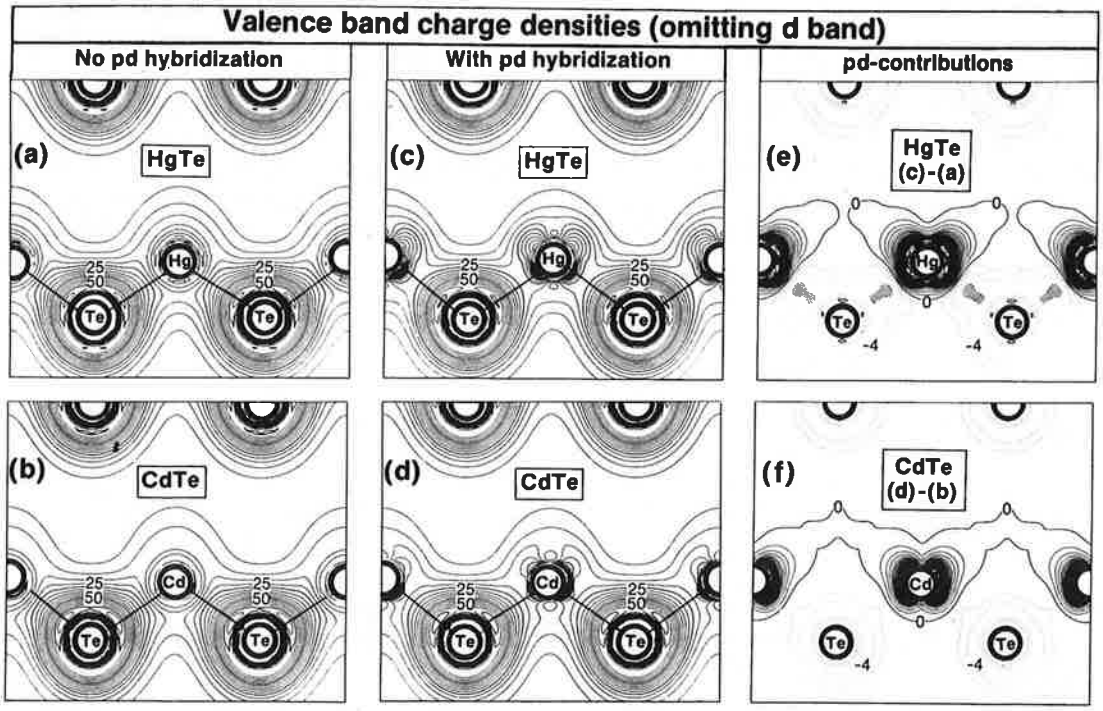


FIG. 6. Comparison of charge density of CdTe and HgTe valence states calculated in (a) and (b) without $p$–$d$ hybridization and in (c) and (d) with $p$–$d$ hybridization (see text). (e) and (f) show the corresponding charge density differences. For clarity of display the cation $d$ bands were omitted. Note in (e) how $p$–$d$ hybridization removes charge from the Hg–Te bond. The charge density is given in units $[10^{-3}\,\mathrm{e}/(\mathrm{a.u.})^3]$. The step sizes are five in (a)–(d) and two in (e)–(f). The dashed lines indicate negative region. The reduced bond strength in (e) is highlighted by the shaded area.

If $p$–$d$ mixing is allowed, the spin–oribt splitting can be described[59] as a linear combination of the splittings for pure $p$ and pure $d$ orbitals $\Delta_p$ and $\Delta_d$, weighed by the fraction $Q_d$ of the $d$ charge in the state of question, i.e.,

$$\Delta \simeq \alpha(1-Q_d)\Delta_p + \beta Q_d \Delta_d, \tag{4}$$

where $\alpha$ and $\beta$ are the geometrical coefficient depends on the charge distribution of the state. In CuCl, having a very strong $p$–$d$ mixing, $\Delta_0$ is *negative*.[35]

We have calculated the spin–orbit splitting $\Delta_0$ at $\Gamma_{15v}$ and $\Delta_1$ at $L_{3v}$ directly from the band structure through a second variation procedure.[39(b)] The results [$\Delta_0$ (band calculation) and $\Delta_1$ (band calculation)] are given in Table IV. In addition, we have calculated $\Delta_0$ and $\Delta_1$ from Eq. (4). We find that if we consider $\Delta_p$ as the SO splitting of the $\Gamma_{15v}$ states with no $pd$ hybridization and $\Delta_d$ as the SO splitting of the cation $d$ states then the coefficients $\alpha$ and $\beta$ of Eq. (4) satisfy approximately $\alpha(1-Q_d)\simeq\beta\simeq 1$, i.e.,

$$\Delta = \Delta_p + Q_d\Delta_d. \tag{5}$$

Results obtained using this equation are also given in Table IV {denoted $\Delta$ [Eq. (5)]}. Our basic conclusions are the following: (i) Using in Eq. (5) the fraction of $d$ character ($Q_d$) obtained from band-structure calculations we reproduce nearly the same spin–orbit splitting obtained directly by incorporating the spin–orbit operator $H_{SO}$ into the band Hamiltonian. (ii) Our LAPW results are in substantial agreement with the LMTO results of Refs. 50 and 51. (iii) Our calculated results agree reasonably with experiment (Table III) for ZnTe and CdTe, but disagree with the experimental value[57,61–68] quoted for HgTe (Table III). (iv) If $p$–$d$ coupling is neglected (resulting in the $\Delta_0 = \Delta_p$; values given in the first line of Table IV), we find better agreement with the current experimental data for HgTe.

The disagreement with the experimental result for HgTe deserves further attention. The experimental measurement of $\Delta_0$ for HgTe is complicated by the inverted band structure of this compound [see Fig. 2(c), showing $\Gamma_{1c}$ *below* $\Gamma_{15v}$]. Unfortunately, only *indirect* measurements[61–68] have been used to deduce $\Delta_0$ for HgTe. On the theoretical side, two uncertainties exist. First, in calculating $\Delta_0$ from the band structure we assumed that the $j=l+1/2$ and $j=l-1/2$ radial orbitals can be averaged.[39] This approximation could introduce an error of $\leqslant 0.2$ eV for the Hg $6p_{1/2}$ state, hence the spin–orbit splitting of the Hg $6p$ level is underestimated by this amount. Since the $\Gamma_{15v}$ valence-band maximum of HgTe includes but 6% Hg $6p$ character, the value of $\Delta_0$ is underestimated by $\leqslant 0.02$ eV. This correction can be added to our directly calculated value of Table IV. The second potential source of error in the theory may arise from the fact that the calculated $d$ band energies (Table III) are less bound than photoemission studies indicate (Table I); hence, $p$–$d$ hybridization is overestimated in our calculation. To examine quantitatively the effects of this error, we have repeated a series of self-consistent band-structure calculations for ZnTe, CdTe, and HgTe, artificially moving the cation $d$ bands to deeper binding energies. (This was done by artificially increasing the exchange parameter $\alpha$ which multiplies the exchange potential away from its nominal value of $\frac{2}{3}$ towards 1. Owing to the larger spatial localization of cation $d$ orbitals relative to all other valence states, this scaling moves the cation $d$ bands to more negative energies relative to other states.) Figure 7 depicts the calculated $\Delta_0$ for ZnTe, CdTe, and HgTe as a function of the separation of the cation $d$ band from the valence band maximum. The vertical arrows denote the observed position of the $d_{3/2}$ states in photoemission experiments (Table I). Adding the estimated correction due to averaging the $l+1/2$ and $l-1/2$ radial orbitals for HgTe, we find the calculated $\Delta_0$ and $\Delta_1$ values (in eV) at the *observed* position of the cation $d$ bands to be

$$\begin{aligned} &\Delta_0(\mathrm{ZnTe}) = 0.94, \quad \Delta_1(\mathrm{ZnTe}) = 0.56; \\ &\Delta_0(\mathrm{CdTe}) = 0.91, \quad \Delta_1(\mathrm{CdTe}) = 0.56; \\ &\Delta_0(\mathrm{HgTe}) = 0.90, \quad \Delta_1(\mathrm{HgTe}) = 0.63; \end{aligned} \tag{6}$$

hence,

$$\Delta_0(\mathrm{CdTe}) \simeq \Delta_0(\mathrm{HgTe}), \tag{7}$$

TABLE IV. Calculated spin–orbit splittings at $\Gamma$ (denoted $\Delta_0$) and $L$ (denoted $\Delta_1$), in eV. $Q_d$ denotes the fraction of $d$ character in the respective wave functions. $\Delta$ (band calc.) is the value obtained from direct band-structure results, using the approach of Ref. 39. $\Delta$ [Eq. (5)] corresponds to the simple approximation of Eq. (5) where the SO splitting is expressed as a combination of the $p$-orbital contributions $\Delta_p$ and the $d$-orbital contribution $Q_d\Delta_d$. Here $\Delta_p$ is obtained from band calculations at $\Gamma_{15v}$ where $p$–$d$ repulsion is omitted, and $\Delta_d$ is obtained as the splitting of the cation $d$ state when $p$–$d$ repulsion is included. $\Delta_d$ is very close to the value obtained from atomic calculation, which gives $-0.35$, $-0.70$, and $-1.78$ eV for Zn, Cd, and Hg, respectively.

| | ZnTe | CdTe | HgTe |
|---|---|---|---|
| $\Delta_p$ ($\Gamma_{15v}$) | 0.92 | 0.90 | 0.99 |
| $\Delta_d$ | −0.37 | −0.69 | −1.68 |
| $Q_d$ ($\Gamma_{15v}$) | 0.072 | 0.074 | 0.129 |
| $\Delta_0$ [Eq. (5)] | 0.89 | 0.85 | 0.78 |
| $\Delta_0$ (band calc.) | 0.89 | 0.86 | 0.78 |
| $\Delta_p$ ($L_{3v}$) | 0.54 | 0.56 | 0.69 |
| $Q_d$ ($L_{3v}$) | 0.045 | 0.045 | 0.085 |
| $\Delta_1$ [Eq. (5)] | 0.52 | 0.53 | 0.55 |
| $\Delta_1$ (band calc.) | 0.51 | 0.53 | 0.53 |

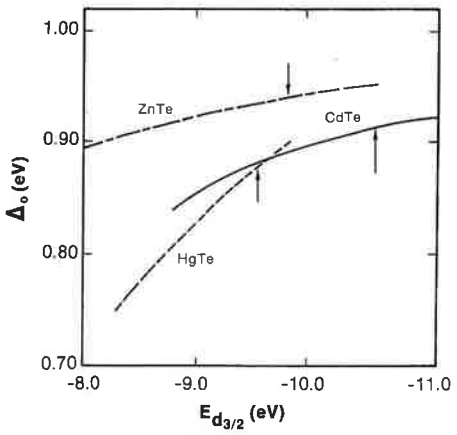


FIG. 7. Variation of spin–orbit splitting $\Delta_0$ as a function of the energy position of the cation $d_{3/2}$ states $E_{d_{3/2}}$ with respect to VBM for ZnTe, CdTe, and HgTe. The arrows point to the position of the experimentally observed $E_{d_{3/2}}$ from photoemission (Table I).

in contrast with the currently accepted experimental results[56,57] $\Delta_0(\mathrm{HgTe}) = 1.08$ eV; $\Delta_0(\mathrm{CdTe}) = 0.90$ eV.

The difference between our predictions of Eq. (7) and the currently accepted experimental values showing $\Delta_0(\mathrm{CdTe}) < \Delta_0(\mathrm{HgTe})$ has an important implication: current interpretations and fittings of $\Delta_0$ have traditionally assumed that $\Delta_0$ of common-anion systems generally increases with the cation atomic number.[60] We find, however, that if $p$–$d$ mixing exists, the opposite can be true, because the conventional analysis disregards $p$–$d$ mixing effects which also increase with the cation atomic number and contribute to a *reduction* of $\Delta_0$. *Direct* experimental determinations of $\Delta_0$ for HgTe would be very desirable and would test our predictions [Eq. (7)], currently in conflict with the indirectly measured $\Delta_0$ values.

### D. Charge redistribution in forming ternary compounds

Current interest in HgTe–CdTe alloys has raised the question of the stability and relative charge transfer[25,26,49] in ordered $\mathrm{Hg}_n\mathrm{Cd}_{4-n}\mathrm{Te}_4$ compounds ($n = 1$, 2, and 3) relative to the binary constituents ($n = 0$ and $n = 4$). We have calculated the band structure, total energies, and charge densities of $\mathrm{HgCdTe}_2$ ($n = 2$ above) in the tetragonal CuAuI-like structure. As discussed in Sec. IV A, we find this ternary compound to have a higher energy per bond relative to its constituents and hence predict that no spontaneous ordering would occur in $\mathrm{Hg}_{0.5}\mathrm{Cd}_{0.5}\mathrm{Te}$ solid solution. To examine the charge redistribution in the ternary compound relative to the binary constituents, we show charge-density differences in Fig. 8 along the bond directions. If the contributions of the cation $d$ bands to the charge densities were ignored [Figs. 8(a) and 8(b), denoted "no $d$") one would have erroneously concluded that in the ternary phase electron charge is *accumulated* on the Hg–Te bond [positive dashed areas in Fig. 8(a)] and *depleted* from the Cd–Te bond [negative dashed areas in Fig. 8(b)]. However, this "weakening" of the Hg–Te bond (relative to the Cd–Te bond) in the ternary system is but an artifact of the omission of the contributions of the cation $d$ bands to the charge densities, as evidenced by Figs. 8(c) and 8(d), exhibiting *depletion* of bond charge on the Hg–Te bond [Fig. 8(c)] and the Cd–Te bond [Fig. 8(d)] in forming the ternary phase from its binary constituents. The buildup of charge on the Hg–Te bond in the absence of contributions from the deep $d$ band [Fig. 8(a)] is merely a consequence of a smaller $p$–$d$ repulsion in $\mathrm{CdHgTe}_2$ relative to HgTe. The reduced bond charge on the Hg–Te bond in the real system [Fig. 8(c)] is due to reduced $d$ orbital bonding in the ternary phase. Using the tight-binding method (which neglects cation $d$ bands) Chen *et al.*[26(b)] have suggested that the reduced Hg–Te bond strength in the ternary is due to an unfavorable charge transfer from Cd–Te bond (in bonding state) to Hg–Te bond (in antibonding state), i.e., in opposite direction to what our calculations show. Their argument is hence, not supported by our results, since we find that charge on the Hg–Te bond is actually *reduced* [Fig. 8(c)].

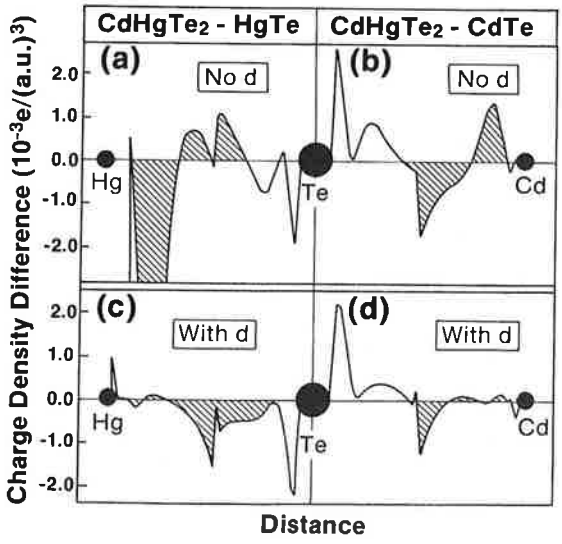


FIG. 8. Valence charge difference between $\mathrm{CdHgTe}_2$ and its binary constituents CdTe and HgTe along the cation–anion bond directions. (a) and (c) Hg–Te bond; (b) and (d) Cd–Te bond. In (a) and (b) cation $d$ bands are removed, in (c) and (d) cation $d$ bands are included.

### E. Valence-band offsets between II–VI compounds

Tight-binding models[69] have calculated the valence-band offset $\Delta E_{\mathrm{vbm}}$ between two semiconductors as the difference between the energies of the $\Gamma_{15v}$ valence-band maximum [Eq. (3)] of AC and BC:

$$E_{\mathrm{vbm}}(\mathrm{AC/BC}) = \epsilon_{\mathrm{BC}}[\Gamma_{15v}] - \epsilon_{\mathrm{AC}}[\Gamma_{15v}]. \quad (8)$$

Since common-anion semiconductors have the same anion energy $\epsilon_p^a$, the difference $\Delta E_{\mathrm{vbm}}$ (AC/BC) reflects in this model the effect of different cation energies $\epsilon_p^c$ and different matrix elements $V_{pp}$. However, all IIB cations have similar $\epsilon_p^c$ values.[22] Furthermore, the CdTe–HgTe and GaAs–AlAs pairs have also nearly identical bond lengths, hence $V_{pp}$ (which, in the tight-bonding model[22(a)] depends solely on bond length) is nearly identical for each member of the pair. This has led, by Eq. (8) to very small $\Delta E_{\mathrm{vbm}}$ (AC/BC) values for most common-anion semiconductors (Table V). This result has been formulated earlier in the hitherto successful "common-anion rule" stating that two semiconductors sharing the same anion would have a very small valence-band offset.

Consider first two binary common-anion semiconductors AX and BX and neglect the effect of $d$ states on the band discontinuity between them [Fig. 9(a)]. The cation $p$ orbitals (A,$p$) and (B,$p$) can couple with the anion $p$ orbital (X,$p$) as all have the same symmetry ($t_2$, or $\Gamma_{15}$) in the zinc-blende lattice. This coupling results in the two bonding states $\Gamma_{15v}$(A–X) and $\Gamma_{15v}$(B–X) whose energy difference provides in this model $\Delta E_v$(AX/BX). We see that each of these bonding states is repelled to *deeper* energies relative to (X,$p$) since the cation $p$ orbital energy is *above* the anion $p$ orbital energy. This repulsion $V(\mathrm{A},p;\mathrm{X},p)^2/[\epsilon(\mathrm{A},p) - \epsilon(\mathrm{X},p)]$ is proportional to the coupling matrix element $V(\mathrm{A}p;\mathrm{X}p)$ and hence increases as the A–X bond length becomes shorter. If AX and BX have the same bond length and similar cation $p$ energies (as is the case in CdTe–HgTe or AlAs–GaAs) this

TABLE V. Calculated and observed valence-band offsets (in eV), for II–VI semiconductor pairs. The right-hand compound in each pair has the higher VBM. Comparison is given with the tight-binding (TB) and Tersoff's results.

| | CdTe/ZnTe | CdTe/HgTe | ZnTe/HgTe | MnTe/CdTe |
|---|---|---|---|---|
| $\Delta E_{\rm VBM}$ (with $d$)[a] | $0.13 \pm 0.02$ | $0.37 \pm 0.03$ | $0.26 \pm 0.04$ | $0.25 \pm 0.10$[b] |
| Expt. | $0.10 \pm 0.06$[c] | $0.35 \pm 0.06$[d]<br>$0.36 \pm 0.05$[c] | $0.25 \pm 0.05$[c] | $<0.1$[e] |
| $\Delta E_{\rm VBM}$ (TB, no $d$)[f] | $-0.07$ | 0.00 | 0.07 | 0.04 |

[a] Present study; spin–orbit splitting effects are included; see Ref. 70.
[b] Averaged over spin-up and spin-down states.
[c] Reference 73.
[d] Reference 72.
[e] Reference 74.
[f] Reference 75 and Eq. (8).

In many binary materials AX and BX the cation $d$ states cannot be neglected. If these orbitals are *below* the anion $p$ state (e.g., Cu 3$d$, Zn 3$d$, Ag 4$d$, Cd 4$d$, Au 5$d$, or Hg 5$d$) they will repel *upwards* the valence-band maximum, as shown in Fig. 9(b). Since this repulsion is proportional to $V(\mathrm{A},d;\mathrm{X},p)^2/[\epsilon(\mathrm{A},d) - \epsilon(\mathrm{X},p)]$ it is larger the shorter the A–X bond is and the shallower is the $d$ orbital energy of the cation A. Hence, since the Hg 5$d$ state is shallower than the Cd 4$d$ state, HgTe would have a *higher* VBM energy than CdTe. This model leads to finite band offsets between common-anion pairs with the same bond length and similar cation $p$ orbital energies, in agreement with experiment. (Note that Al has empty, high-energy 3$d$ orbitals which *lower* the VBM in AlAs relative to GaAs.)

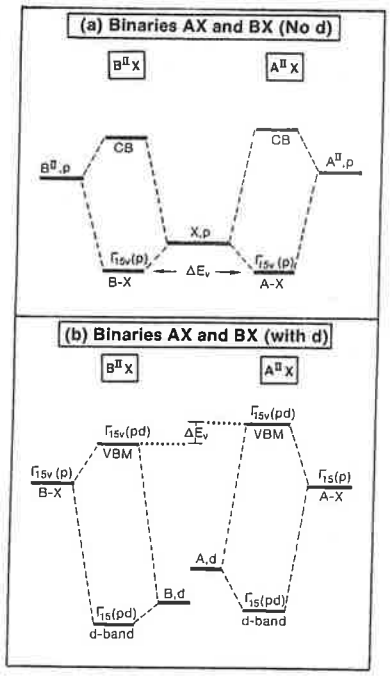


FIG. 9. Energy level diagram applied to binary semiconductor heterojunctions, neglecting (a) or considering (b) the role of the cation $d$ states. CB indicates conduction band.

We have calculated[70,71] the valence-band offsets of the four common-anion semiconductors CdTe/HgTe, CdTe/ZnTe, ZnTe/HgTe, and MnTe/CdTe in a way that parallels their measurement in photoemission core level spectroscopy.[72] Three quantities are needed in such a calculation. The core level binding energies $E^{\rm AC}_{nl,\rm A}$ and $E^{\rm BC}_{n'l',\rm B}$ of the cations A and B, respectively, relative to the VBM (obtained from the band structures of AC and BC, respectively) and the core level difference $\Delta E^{\rm A,B}_{nl,n'l'}$ [calculated from the band structure of the (001) $(\mathrm{AC})_1(\mathrm{BC})_1$ superlattice, which is equivalent to the $\mathrm{ABC}_2$ "CuAu-I" structure]. We have shown,[71] using a simple electrostatic model, that for common-anion systems interface dipole effects can be small and localized near the interface, so that an ultrathin superlattice could be used to obtain the core level difference $\Delta E^{\rm A,B}_{nl,n'l'}$. The valence-band offset $\Delta E_{\rm VBM}$ is then obtained as

$$\Delta E_{\rm VBM} \cong E^{\rm AC}_{nl,\rm A} - E^{\rm BC}_{n'l',\rm B} + \Delta E^{\rm A,B}_{nl,n'l'}. \tag{9}$$

We find that after including $p$–$d$ hybridization our calculated valence-band offsets are in good agreement with experimental data. Our results (with $d$) are compared with tight-binding (TB) calculation (no $pd$ repulsion) and experimental data for CdTe/ZnTe, CdTe/HgTe, ZnTe/HgTe, and MnTe/CdTe in Table V.[72–75]

## F. Alloy clustering and stability of inter-II–VI compounds

One of the central quantities computed in statistical mechanics models of $\mathrm{A}_x\mathrm{B}_{1-x}\mathrm{C}$ alloys,[48,49,76] is the populations of the C-centered molecular clusters $\mathrm{A}_n\mathrm{B}_{4-n}$ $(0 \leqslant n \leqslant 4)$ at given compositions $(x)$ and temperatures $(T)$. These cluster populations, $P^{(n)}(x,T)$ are then contrasted with those predicted by a purely random $(R)$ distribution $P^{(n)}_R(x)$. If

$$\Delta P^{(n)}(x,T) = P^{(n)}(x,T) - P^{(n)}_R(x) \tag{10}$$

is positive, the system is said to exhibit "clustering" of cluster $n$, whereas if $\Delta P^{(n)}(x,T) < 0$, it is said to exhibit "anti-clustering." These quantities depend naturally on the volume-dependent interaction energies $\Delta E^{(n)}(V)$ of the $\mathrm{A}_n\mathrm{B}_{4-n}\mathrm{C}_4$ (free or embedded) clusters,

$$\Delta E^{(n)}(V) = E[A_nB_{4-n}C_4;V] - (n/4)E[AC] - [(4-n)/4]E[BC]. \quad (11)$$

Figure 10 contrasts the cluster energies obtained by Sher *et al.*[49] with those obtained here for the $Hg_{1-x}Cd_xTe$ system. The tight-binding results [Fig. 10(a)] predict that the $Hg_2Cd_2Te_4$ cluster is stable relative to its constituents [$\Delta E^{(2)} < 0$], whereas our first-principles results [Fig. 10(b)] show the opposite. Furthermore, Sher *et al.* predict the $HgCd_3$ and $Hg_3Cd$ clusters to have comparable excess energies and that both are less stable than $Hg_2Cd_2$, whereas the present results predict the 1:3 clusters to be stabler then the 1:1 cluster. Figure 11 contrasts the excess populations $\Delta P^{(n)}(x,T)$ obtained by both groups, using the quasichemical method in the case of Sher *et al.*,[49,76] and the cluster variation method[48] in the present study. Table VI compares the signs of $\Delta P^{(n)}(x,T)$ obtained with the various methods, compared with those deduced from recent nuclear magnetic resonance (NMR) studies.[77–79] We see the following: (i) For the alloy systems $Hg_{1-x}Zn_xTe$ and $Cd_{1-x}Zn_xTe$ (for which a considerable size mismatch exists between the binary constituents), the tight-binding theory[49,76] predicts an incorrect sign of $\Delta P^{(n)}(x)$ for all cases where data are available. (The present first-principles theory has not been extended yet to these systems.) (ii) For $Hg_{1-x}Cd_xTe$ (nearly vanishing size mismatch), the present theory and tight binding agree on the sign of $\Delta P^{(n)}(x,T)$ for $n \neq 2$ (but not for $n = 2$ in Hg-rich side). Both theories agree with experiment for Hg-poor alloys, and both disagree with experiment (which suggests a deficiency of $Hg_4Te$ clusters) for Hg-rich alloys.

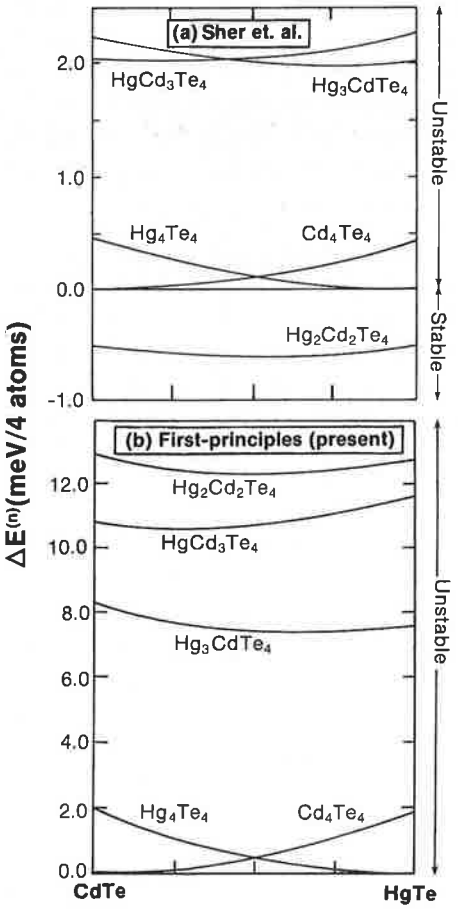


FIG. 10. Calculated excess cluster energies [Eq. (11)] for $Hg_nCd_{4-n}Te_4$. Results of Sher *et al.* (Ref. 49) are shown in (a), whereas (b) shows the present first-principles results.

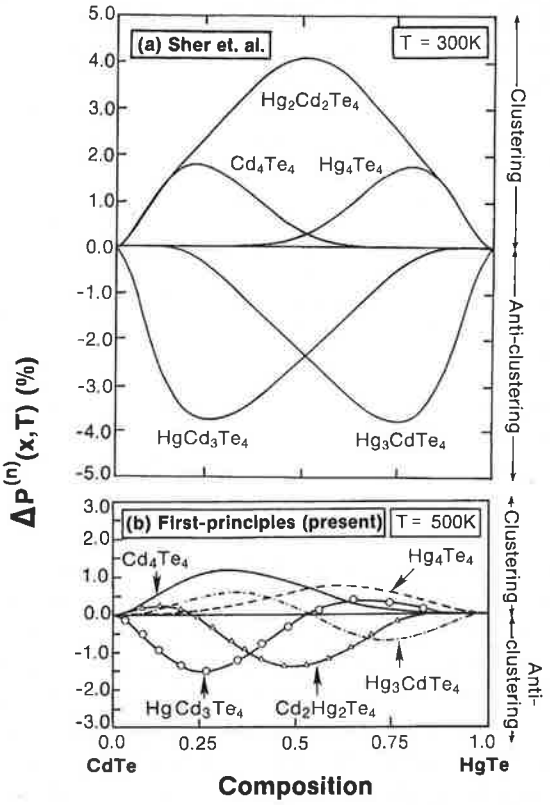


FIG. 11. Calculated excess cluster probabilities [Eq. (10)] for CdTe–HgTe alloys. The results of Sher *et al.* (Ref. 49) are shown in (a), whereas (b) gives the present first-principles results.

The discrepancies between theory and experiment for Hg-rich $Hg_{1-x}Cd_xTe$ alloys deserve further attention. It is possible that the Hg-rich samples[78] were structurally poor, i.e., that not all of the nominal Hg was actually bonded to Te in the fcc lattice, but a portion of it existed as metallic inclusions or as a surface segregated phase, or has been lost altogether from the sample. Hence, the experimental result suggesting deficiency of *bonded* $Hg_4Te$ clusters could reflect the fact that not all 75% Hg are bonded to Te. There are two experimental facts that support this possibility. First, Trekhov *et al.*[80(a)] have observed that one needs a nominal $Cd_{0.45}Hg_{0.55}Te$ sample to maintain an equal number of Cd and Hg atoms on the cation sublattice, i.e., a nominal $x = 0.5$ sample has $< 50\%$ *bonded* Hg. Second, Sporken *et al.*,[80(b)] in studying the Hg core photoemission have found that a substantial amount of Hg outdiffuses from the sample to its surface, leaving a deficiency of $Hg_4Te$ in the bulk and producing cluser $Hg_n$ *on* the surface (with radii of 5–10 Å) of the sample. The Hg $4f_{7/2}$ photoemission of the surface-clustered Hg appears at a higher binding energy than that of the bulk Hg. For large cluster radii $R$, the binding energy of

TABLE VI. Comparison between theory and experiment in the predicted trends in clustering [Eq. (10)].

| Cluster type | Hg-rich $Hg_{1-x}Zn_xTe$ | | Hg-poor $Hg_{1-x}Zn_xTe$ | |
|---|---|---|---|---|
| | Sher *et al.*[a] | Exptl. | Sher *et al.*[a] | Exptl. |
| $Hg_4$ | Deficiency ( − ) | | | |
| $Hg_3Zn$ | Excess ( + ) | | | |
| $HgZn_3$ | Deficiency ( − ) | | Excess ( + ) | |
| $Zn_4$ | | | Deficiency ( − ) | |
| | Cd-rich $Cd_{1-x}Zn_xTe$ | | Cd-poor $Cd_{1-x}Zn_xTe$ | |
| Cluster type | Sher *et al.*[b] | Exptl.[c] ($x \leqslant 0.12$) | Sher *et al.*[a] | Exptl.[c] ($x = 0.9$) |
| $Cd_4$ | Deficiency ( − ) | Excess ( + ) | | |
| $Cd_3Zn$ | Excess ( + ) | Deficiency ( − ) | | |
| $CdZn_3$ | Deficiency ( − ) | | Excess ( + ) | Deficiency ( − ) |
| $Zn_4$ | | | Deficiency ( − ) | Excess ( + ) |
| | Hg-rich $Hg_{1-x}Cd_xTe$ | | | Hg-poor $Hg_{1-x}Cd_xTe$ |
| Cluster type | Sher *et al.*[d] | Wei and Zunger | Exptl.[e] ($x = 0.25$) | Sher *et al.*[d] | Wei and Zunger | Exptl.[d] ($x = 0.75$) |
| $Hg_4$ | Excess ( + ) | Excess ( + ) | Deficiency ( − ) | | | |
| $Hg_3Cd$ | Deficiency ( − ) | Deficiency ( − ) | Excess ( + ) | | | |
| $Hg_2Cd_2$ | Excess ( + ) | Deficiency ( − ) | | Excess ( + ) | Excess ( + ) | |
| $HgCd_3$ | | | | Deficiency ( − ) | Deficiency ( − ) | Deficiency ( − ) |
| $Cd_4$ | | | | Excess ( + ) | Excess ( + ) | Excess ( + ) |

[a] Results for clustering in $Hg_{1-x}Zn_xTe$ were presented by Sher *et al.* in Ref. 49, Fig. 5. Note that the labels for $Hg_4$ and $Zn_4$ were interchanged erroneously in this figure. The same error occurred in Fig. 5 of Sher *et al.* (Ref. 76).

[b] Results for clustering in $Cd_{1-x}Zn_xTe$ were presented by Sher *et al.*, Ref. 76, Fig. 4. Note that the labels for $Cd_4$ and $Zn_4$ were erroneously interchanged in this figure.

[c] Beshah *et al.*, Ref. 77.

[d] Results for clustering in $Hg_{1-x}Cd_xTe$ were presented by Sher *et al.*, Ref. 49, Fig. 6. Note that the labels $Hg_4$ and $Cd_4$ were erroneously interchanged in that figure.

[e] Zax *et al.*, Ref. 78.

the surface Hg approaches that of metallic Hg. This raises the possibility that the Hg-rich samples studied by NMR contain less bulk bonded Hg than the nominal concentration would suggest, explaining the discrepancy with theory. A careful reexamination of the content of the *bonded* Hg in this sample and new experiments on crystalline samples (rather than crushed polycrystalline samples of unknown stoichiometry[78]) are called for.

## G. Ground-state properties of ordered alloys

To assess the relative stability of the various bonds between II–VI compounds, we have calculated the total energies of ordered $A_nB_{4-n}C_4$ structures (zinc blende for $n = 0$ and 4, the tetragonal CuAuI-like structure for $n = 2$ and the "Luzonite" structure for $n = 1$ and 3). The total energy has been minimized both with respect to the lattice parameter and with respect to the cell-internal structural degrees of freedom, controlling the two bond lengths $R$(A–C) and $R$(B–C) and the bond angles. We define the formation enthalpy $\Delta H^{(n)}$ of the structure $A_nB_{4-n}C_4$ as its energy (at equilibrium) with respect to the energies of equivalent amounts of AC and BC (also at their equilibrium) [i.e., as the equilibrium value of Eq. (11)]:

$$\Delta H^{(n)} = E[A_nB_{4-n}C_4; V_{eq}] - (n/4)E[AC] - [(4-n)/4]E[BC]. \quad (12)$$

Table VII gives $\Delta H^{(n)}$ in units of kcal per four-atom formula mole (i.e., $ABC_2$, or double zinc blende). Table VII also gives the bulk moduli $B^{(n)}$, the equilibrium bond lengths, and the dimensionless parameter $u$ measuring the extent of bond alternation in these systems. For the CuAuI structure, assuming $c = a$, we have

$$R(\text{A–C}) = [1/8 + u^2]^{1/2}a,$$
$$R(\text{B–C}) = [1/8 + (1/2 - u)^2]^{1/2}a, \quad (13)$$

for the Luzonite structure ($AB_3C_4$, space group $T_d^1$), we have

$$R(\text{A–C}) = \sqrt{3}ua,$$
$$R(\text{B–C}) = [2(1/2 - u)^2 + u^2]^{1/2}a, \quad (14)$$

so that $u = 1/4$ gives $R$(A–C) = $R$(B–C). The results show the following:

(i) In all cases, $\Delta H^{(n)} > 0$, hence the ternary ordered phase $A_nB_{4-n}C_4$ for $n = 1$, 2, or 3 will disproportionate, at equilibrium, to $n$AC + (4 − $n$)BC. (This is reflected by the increased population of $Hg_4$ and $Cd_4$ clusters in Fig. 11.)

TABLE VII. Calculated (semirelativistic LAPW) ground-state properties of ordered $A_nB_{4-n}C_4$ ($0 \leqslant n \leqslant 4$) structures between ZnTe, CdTe, and HgTe.

| Ordered compound | $a_{eq}^{(n)}$ (Å) | $R$(Zd–Te) (Å) | $R$(Cd–Te) (Å) | $R$(Hg–Te) (Å) | $u$ | $B^{(n)}$ (GPa) | $\Delta H^{(n)}$ (kcal/4-atom mole) |
|---|---|---|---|---|---|---|---|
| ZnTe | 6.052 | 2.621 | ··· | ··· | 0.25 | 52.1 | 0 |
| CdTe | 6.470 | ··· | 2.802 | ··· | 0.25 | 44.0 | 0 |
| HgTe | 6.492 | ··· | ··· | 2.811 | 0.25 | 46.1 | 0 |
| $Cd_3ZnTe_4$ | 6.368 | 2.643 | 2.797 | ··· | 0.2397 | 47.3 | 0.76 |
| $CdZnTe_2$ | 6.263 | 2.638 | 2.790 | ··· | 0.2290 | 44.0 | 1.25 |
| $CdZn_3Te_4$ | 6.158 | 2.630 | 2.783 | ··· | 0.2609 | 50.2 | 1.08 |
| $Hg_3ZnTe_4$ | 6.383 | 2.645 | ··· | 2.806 | 0.2393 | 48.6 | 0.62 |
| $HgZnTe_2$ | 6.269 | 2.637 | ··· | 2.797 | 0.2279 | 45.2 | 0.98 |
| $HgZn_3Te_4$ | 6.163 | 2.632 | ··· | 2.787 | 0.2611 | 49.4 | 0.84 |
| $Cd_3HgTe_4$ | 6.476 | ··· | 2.802 | 2.810 | 0.2505 | 44.8 | 0.24 |
| $CdHgTe_2$ | 6.481 | ··· | 2.801 | 2.812 | 0.2485 | 44.2 | 0.28 |
| $CdHg_3Te_4$ | 6.485 | ··· | 2.804 | 2.810 | 0.2496 | 46.2 | 0.17 |

Our results for $HgCdTe_2$ disagree with the results of Sher *et al.*[49] and Hass and Vanderbilt[20] who found that if the (destabilizing) $d$ band is ignored, $\Delta H[CdHgTe_2] < 0$.

(ii) Comparing the magnitudes of $\Delta H^{(n)}$ for a fixed stoichiometry $n$ and different compounds (e.g., $CdHgTe_2$, $HgZnTe_2$, and $CdZnTe_2$) we find that $CdHgTe_2$ (having a very small lattice mismatch between its binary constituents) is the least unstable, whereas both $HgZnTe_2$ and $CdZnTe_2$ (with relative lattice mismatches of 5.9% and 6.2%, respectively) are considerably less stable. (Of course, formation enthalpies reflect thermodynamic stability/instability towards disproportionation, not to be confused with stability against *other* reactions, such as oxidation, diffusion, etc.) Our results are in generally good agreement with the pseudopotential calculation[20] for lattice mismatched $CdZnTe_2$ and $HgZnTe_2$. Tight-binding calculation by Sher *et al.*[76] give $\Delta H[Hg_{0.5}Zn_{0.5}Te] \simeq 0.72$ kcal/(4-atom mole) and $\Delta H[Cd_{0.5}Zn_{0.5}Te] \simeq 0$ [Fig. 3(a) and 3(b), Ref. 76], however, results given by Sher *et al.* in Ref. 25 show $\Delta H[Cd_{0.5}Zn_{0.5}Te] \simeq 0.65$ kcal/(4-atom mole).

(iii) We find that the shorter of the two bonds in AC and BC becomes *longer* in the ternary phase $A_nB_{4-n}C_4$, whereas the longer of the two binary bonds becomes shorter. Hence, comparing ZnTe and CdTe, the shorter (Zn–Te) bond has a length of 2.621, 2.630, 2.638, and 2.643 Å in ZnTe, $Cd_3ZnTe_4$, $CdZnTe_2$, and $CdZn_3Te_4$, respectively. This agrees with the valence force field (VFF) calculations of Martins and Zunger[81] and with extended x-ray absorption fine-structure (EXAFS) measurements.[82] In the CdTe–HgTe system (where our theory underestimates the length of the Cd–Te bond by 0.004 Å and overestimates that of Hg–Te by 0.013 Å), we find that the bond lengths in the ternary phase are nearly unchanged relative to their values in the binary compounds (e.g., the Hg–Te bond length is 2.811 Å in HgTe and 2.812 Å in $CdHgTe_2$; the Cd–Te bond length is 2.802 Å in CdTe and 2.801 Å in $CdHgTe_2$). This conflicts with the results of Sher *et al.*[26] and Hass and Vanderbilt[20] who find that the shorter (Hg–Te) bond becomes *substantially shorter* in the ternary phase, whereas the longer (Cd–Te) bond becomes yet longer in the ternary phase. This effect can be quantified by defining the relative bond length mismatch $R_{BC}[A\,C{:}B] - R_{AC}[B\,C{:}A]$ in the dilute *alloy* (or impurity) limit with respect to the size mismatch in the *pure* compounds, $R^0_{BC}$ and $R^0_{AC}$:

$$\eta(x) = (R_{BC}[A_xB_{1-x}C] - R_{AC}[A_{1-x}B_xC])/(R^0_{BC} - R^0_{AC}), \quad (15a)$$

$$\eta(x \to 1) = (R_{BC}[AC{:}B] - R_{AC}[BC{:}A])/(R^0_{BC} - R^0_{AC}). \quad (15b)$$

If $\eta < 1$, the alloy environment acts to *reduce* the difference between the bond lengths of the constituents, whereas if $\eta > 1$, the alloy *amplifies* the difference. For HgCdTe, Chen *et al.*[26] find $\eta(1) \cong 8$ and Hass and Vanderbilt[20] find $\eta(1) \cong 11$, whereas we find for all systems $\eta \leqslant 1$. Since this effect is very large in the calculations neglecting the $d$ bands[20,26] (the Hg–Te and Cd–Te bond lengths are predicted to differ in the $Hg_{0.5}Cd_{0.5}Te$ alloy by 0.05 Å, compared with 0.009 Å in the end-point compounds), if correct it should be readily observed in future EXAFS measurements.

## H. Optical bowing

Our calculations of the electronic structure of $A_nB_{4-n}C_4$ also provides information on their band structure. Bernard and Zunger[83] and Wood *et al.*[84] have shown that the optical bowing parameter $b$ of an $A_xB_{1-x}C$ alloy can be calculated as a sum of an "ordered" contribution $b_{ord}$ (obtained from comparing the band gap of ordered $ABC_2$ in CuAuI structure to the average of the gaps of AC and BC) and a "disordered" contribution $b_{dis}$, reflecting the fact that the $A_xB_{1-x}C$ alloys contains, even at $x = 0.5$, not only the $A_2B_2$ cluster, but also the $A_4$, $A_3B$, $AB_3$, and $B_4$ clusters (Fig. 11):

$$b = b_{ord} + b_{dis}. \quad (16)$$

For systems with a lattice mismatch, it is found that $b_{ord} > b$, hence the "disorder" contribution acts to increase the alloy band gap, *reducing* thereby its bowing parameter.

To calculate the band gaps of the systems of interest here, we must first correct for the well-known[85] underestimation of gaps by the local density approximation (LDA). We do so by contrasting the LDA calculated gaps for ZnTe, CdTe, and HgTe with those measured[35] (extrapolating the result to

TABLE VIII. Band gaps of binary and ternary II–VI compounds.

| | $E_g$ (LDA) (eV) | $E_g$ (exptl.) 0 K (eV) | LDA error (eV) | LDA corrected (eV) | $b$ (exptl. at $x = 0.5$) | $b_{ord}$ (calc. at $x = 0.5$) |
|---|---|---|---|---|---|---|
| ZnTe | 1.02 | 2.39[a] | 1.37 | 2.39 | ... | ... |
| CdTe | 0.47 | 1.61[a] | 1.14 | 1.61 | ... | ... |
| HgTe | −0.99 | −0.30[a] | 0.69 | −0.30 | ... | ... |
| $CdHgTe_2$ | −0.27 | 0.60[b] | (0.91) | 0.64 | 0.23[b],0[a] | 0.05 |
| $HgZnTe_2$ | −0.09 | 1.01[c] | (1.03) | 0.94 | 0.14[c] | 0.41 |
| $CdZnTe_2$ | 0.64 | 1.94[d] | (1.25) | 1.89 | 0.26[d] | 0.44 |

[a] Reference 35.
[b] Alloy data at $x = 0.5$, recommended $T = 0$ K values by Brice, from data compiled in Ref. 86.
[c] Alloy data at $x = 0.5$, Ref. 87.
[d] Reference 88.

0 K), and applying to our calculated LDA gaps of $ABC_2$ the average LDA error for AC and BC (Table VIII). We hence predict for $CdHgTe_2$, $HgZnTe_2$, and $CdZnTe_2$ zero-temperature band gaps of 0.64, 0.94, and 1.89 eV, respectively. The measured results for the corresponding disordered alloys at $x = 0.5$ (extrapolated to 0 K) are 0.595,[86] 1.01,[87] and 1.94 eV,[88] respectively. Our calculated $b_{ord}$, given in Table VIII, overestimates, as discussed above, the total $b$ for lattice mismatched system, yet they suggest definite trends $b(\text{CdZnTe}) \simeq b(\text{HgZnTe}) \gg b(\text{CdHgTe})$ associated with the trends in bond length mismatch[83] (see also Table VII). Our result $b_{ord}$ (CdHgTe) = 0.05 eV can be compared also with that of Podgorny and Czyzyk[29] (0.96 eV), Hass *et al.*[27] (~0.27 eV), and Berding *et al.*[89] (0.36 eV). For HgZnTe, our result $b_{ord}$ (HgZnTe) = 0.41 eV can be compared with $b = 0.79$ eV obtained by Berding *et al.*[89] None of the other calculations incorporate the metal $d$ band. This explains why these approaches *overestimate* the bowing parameters in these systems: Since there is a smaller $p$–$d$ repulsion in $ABC_2$ relative to AC and BC, inclusion of this effect raises the gap of $ABC_2$ (hence, reduces the bowing) relative to calculations which omit $d$ bands.

## V. SUMMARY

We have demonstrated that the existence of a fully occupied, nominally "nonbonding" $d$ band inside the valence band of II–VI semiconductors affects the properties of these systems near the valence-band maximum. The incomplete screening by the $d$ electrons of the core leads to profoundly different properties of IIB–VI compounds relative to IIA–VI compounds, lacking this $d$ shell. In addition, the $d$ electrons have a *direct* effect on the other orbitals of the system, due to the symmetry-allowed $p$–$d$ interaction. These effects involve (i) reduction of the direct band gap due to upward repulsion of the $\Gamma_{15v}$ state by the $d$ bands at lower energies; (ii) reduction of the spin–orbit splitting; (iii) reversal of the order of the $d$-orbital $\Gamma_{15}$ and $\Gamma_{12}$ states relative to the prediction of point–ion crystal-field models; (iv) introduction of antibonding character in the charge distribution of the upper valence bands; (v) significant increase in the valence-band offset between common-anion II–VI pairs (e.g., CdTe–HgTe); and (vi) reduction in the optical bowing parameters.

We further predict that $p$–$d$ repulsion will lead to a near equality of the spin–orbit splitting at $\Gamma_{15v}$ of CdTe and HgTe, in contrast with the currently accepted result $\Delta_0$ (HgTe) > $\Delta_0$ (CdTe). Detailed results on equilibrium bond lengths, formation enthalpies, and clustering of inter-II–VI compounds are presented.

*Note added in proof*: In Sec. IV G we have shown that whereas calculations omitting the $d$ bands (Refs. 20, 26) predict that the alloy environment in $Hg_{1-x}Cd_xTe$ acts to *increase* the bond length size difference $R_{\text{Cd-Te}}(x) - R_{\text{Hg-Te}}(x)$ relative to the same quantity $R_{\text{Cd-Te}}(1) - R_{\text{Hg-Te}}(0)$ in the pure end-point compounds, our own calculations predict the opposite, i.e., that $\eta(x)$ of Eq. (15a) satisfies $\eta(x) \leqslant 1$. Recently, an experimental EXAFS study of the bond lengths in $Hg_{1-x}Cd_xTe$ has been published by Balzarotti [Physica B **146**, 150 (1987)]. This shows that $R^0_{\text{Hg-Te}}(0) = 2.798$ Å, $R^0_{\text{Cd-Te}}(1) = 2.8065$ Å, $R_{\text{Hg-Te}}(0.5) = 2.799$ Å, and $R_{\text{Cd-Te}}(0.5) = 2.803$ Å, yielding $\eta(0.5) = 0.47$. Although small uncertainties in the (rather close) bond lengths of the end-point compounds are critical for the EXAFS analysis, this experimental study seems to clearly demonstrate that the alloy environmental *reduces* the bond length size mismatch (i.e., the long bond becomes shorter and the short bond becomes longer), in agreement with our prediction [$\eta(0.5) \simeq 1$ from our Table VII], and in conflict with the previous no-$d$ calculations[20,26] [e.g., $\eta(0.5) \simeq 5.8$ in Ref. 20 and $\eta(0.5) \simeq 4.4$ in Ref. 26]. This new experimental result also contradicts the speculation of Ref. 77 that $\eta(x) > 1$.

## ACKNOWLEDGMENTS

We gratefully acknowledge stimulating discussions with Dr. D. Zamir and Dr. S. Vega on the NMR results for II–VI alloys. This work was supported by the Office of Energy Research, Materials Science Division, U.S. Department of Energy, under Grant No. DE-AC02-77-CH00178.

[1] N. J. Shevchik, J. Tejeda, M. Cardona, and D. W. Langer, Phys. Status Solidi B **59**, 87 (1973).
[2] L. Ley, R. A. Pollak, F. R. Mcfeely, S. P. Kowalczyk, and D. A. Shirley, Phys. Rev. B **9**, 600 (1974).
[3] (a) C. J. Veseley, R. L. Hengehold, and D. W. Langer, Phys. Rev. B **5**, 2296 (1972); (b) E. P. Domashevskaya and V. A. Terehov, Phys. Status Solidi B **105**, 121 (1981); (c) V. Formichev, T. M. Zimkina, and I. I. Zhukovn, Sov. Phys. Solid State **10**, 2421 (1969).

[4]D. J. Stukel, R. N. Euwema, T. C. Collins, F. Herman, and R. L. Kortum, Phys. Rev. **179**, 740 (1969).
[5]F. Herman, R. L. Kortum, C. D. Kuglin, and J. L. Shay, in *II–VI Semiconducting Compounds*, edited by D. G. Thomas (Benjamin, New York, 1967), p. 503; F. Herman, R. L. Kortum, C. D. Kuglin, J. P. Van Dyke, and S. Skillman, in *Methods of Computational Physics* (Academic, New York, 1968), p. 193.
[6]P. Eckelt, O. Madelung, and J. Treusch, Phys. Rev. Lett. **18**, 656 (1967); J. Treusch, P. Eckelt, and O. Madelung, in *II–VI Semiconducting Compounds*, edited by D. G. Thomas (Benjamin, New York, 1967), p. 558; H. Overhof, Phys. Status Solidi B **45**, 315 (1971).
[7]A. Zunger and A. J. Freeman, Phys. Rev. B **17**, 4850 (1978).
[8]C. S. Wang and B. M. Klein, Phys. Rev. B **27**, 3393 (1981).
[9]P. Bendt and A. Zunger, Phys. Rev. B **26**, 3114 (1982).
[10]J. E. Bernard and A. Zunger, Phys. Rev. B **36**, 3199 (1987); **34**, 5992 (1986).
[11]S.-H. Wei and A. Zunger, Phys. Rev. B **35**, 2340 (1987-I).
[12]M. L. Cohen and T. K. Bergstresser, Phys. Rev. **141**, 789 (1966).
[13]M. L. Cohen, in *II–VI Semiconducting Compounds*, edited by D. G. Thomas (Benjamin, New York, 1967), p. 462.
[14]F. Aymerich, F. Meloni, and G. Mulor, Phys. Rev. B **15**, 3980 (1977); F. Aymerich, A. Baldereschi, and F. Meloni, Jpn. J. Appl. Phys. **19**, Suppl. 19-3, 161 (1980).
[15](a) J. R. Chelikowsky and M. L. Cohen, Phys. Rev. B **14**, 556 (1976); (b) R. M. Wentzcovitch, S. L. Richardson, and M. L. Cohen, Phys. Lett. A **114**, 203 (1986); (c) J. R. Chelikowsky, Solid State Commun. **22**, 351 (1977).
[16]J. R. Chelikowsky, D. J. Chadi, and M. L. Cohen. Phys. Rev. B **8**, 2786 (1973).
[17](a) J. D. Joannopoulos and M. L. Cohen, J. Phys. C **6**, 1572 (1973); (b) M. L. Cohen, Science **179**, 1189 (1973); (c) J. P. Walter and M. L. Cohen, Phys. Rev. B **4**, 1877 (1971).
[18](a) J. P. Walter, M. L. Cohen, Y. Petroff, and M. Balkanski, Phys. Rev. B **1**, 2662 (1970); (b) D. J. Chadi, J. P. Walter, M. L. Cohen, Y. Petrokff, and M. Balkanski, Phys. Rev. B **5**, 3058 (1972).
[19](a) J. Ihm and M. L. Cohen, Phys. Rev. B **20**, 729 (1979); W. E. Pickett and M. L. Cohen, *ibid.* **18**, 939 (1978); W. E. Pickett, S. G. Louie, and M. L. Cohen, Phys. Rev. Lett. **39**, 109 (1977); J. R. Chelikowsky and M. L. Cohen, Phys. Rev. B **13**, 826 (1976).
[20]K. C. Hass and D. Vanderbilt, in *18th International Conference on the Physics of Semiconductors*, edited by O. Engstrom (World Scientific, Singapore,1987), pp. 1181; J. Vac. Sci. Technol. A **5**, 3019 (1987).
[21]K. J. Chang, S. Froyen, and M. L. Cohen, Phys. Rev. B **28**, 4736 (1983).
[22](a) W. A. Harrison, *Electronic Structure and the Properties of Solids* (Freeman, San Francisco, 1980); (b) J. Vac. Sci. Technol. B **3**, 1231 (1985).
[23]D. J. Chadi and M. L. Cohen, Phys. Status Solidi B **68**, 49 (1975).
[24]P. Vogl, H. P. Hjalmarson, and J. D. Dow, J. Phys. Chem. Solids **44**, 365 (1983).
[25]A. B. Chen and A. Sher, Phys. Rev. B **32**, 3695 (1985).
[26](a) A. Sher, A. B. Chen, W. E. Spicer, and C. K. Shih, J. Vac. Sci. Technol. A **3**, 105 (1985); (b) A.-B. Chen, A. Sher, and W. E. Spicer, *ibid.* **3**, 1674 (1985).
[27]K. C. Hass, H. Ehrenreich, and B. Velicky, Phys. Rev. B **27**, 1088 (1983).
[28]D. J. Chadi, Phys. Rev. B **16**, 790 (1977); see also D. J. Chadi and M. L. Cohen, *ibid.* **7**, 692 (1973).
[29]M. Podgorny and M. T. Czyzyk, Solid State Commun. **32**, 413 (1974).
[30]A. B. Chen and A. Sher, Phys. Rev. B **31**, 6490 (1985).
[31]P. Pecheur, J. van der Rest, and G. Toussaint, J. Cryst. Growth **72**, 147 (1985); P. H. Meijer, P. Pecheur, and G. Toussaint, Phys. Status Solidi B **140**, 155 (1987).
[32]P. Vogl, in *Festkörperproblem XXI* (Advance in Solid State Physics), edited by P. Grosse (Pergamon/Vieweg, Braunschweig, 1981), p. 191.
[33]H. Watanabe, *Operator Methods in Ligand Field Theory* (Prentice Hall, Englewood Cliffs, NJ, 1966), p. 87.
[34]W. H. Strehlow and E. L. Cook, J. Phys. Chem. Ref. Data **2**, 163 (1973). Results for ZnO are given by D. G. Thomas, J. Phys. Chem. Solids **15**, 86 (1960).
[35]*Landolt-Börnstein Numerical Data and Functional Relationship in Science and Technology*, edited by O. Madelung (Springer, Berlin, 1982), Vol. 17b.
[36]S.-H. Wei and H. Krakauer, Phys. Rev. Lett. **55**, 1200 (1985), and references therein.
[37]P. Hohenberg and W. Kohn, Phys. Rev. B **136**, 864 (1964); W. Kohn and L. J. Sham, Phys. Rev. A **140**, 1133 (1965).
[38]L. Hedin and B. I. Lundqvist, J. Phys. C **4**, 2063 (1971).
[39](a) D. D. Koelling and B. N. Harmon, J. Phys. C **10**, 3107 (1977); (b) A. H. MacDonald, W. E. Pickett, and D. D. Koelling, *ibid.* **13**, 2675 (1980).
[40]R. Juza, A. Rabenau, and G. Pascher, Z. Anorg. Allg. Chem. **285**, 61 (1956).
[41]B. Segall, M. R. Lorenz, and R. E. Halsted, Phys. Rev. **129**, 2471 (1963).
[42]J. C. Wooley and B. Ray, J. Phys. Chem. Solids **13**, 151 (1960).
[43]O. Kubachevski and C. B. Alcock, *Metallurgical Thermochemistry*, 5th ed. (Pergamon, New York, 1979), pp. 267–322.
[44]C. Kittel, *Solid State Physics*, 5th ed. (Wiley, New York, 1976), p. 74.
[45]D. Berlincourt, H. Jaffe, and L. R. Shiozawa, Phys. Rev. **129**, 1009 (1963).
[46]R. Dornhaus and G. Nimitz, in *Narrow-gap Semiconductors*, edited by G. Höhler and E. A. Niekisch (Springer, New York, 1983), p. 126.
[47]A. Fazzio, M. J. Caldas, and A. Zunger, Phys. Rev. B **30**, 3430 (1984).
[48]S.-H. Wei, A. A. Mbaye, L. G. Ferreira, and A. Zunger, Phys. Rev. B **36**, 4163 (1987-I); A. A. Mbaye, L. G. Ferreira, and A. Zunger, Phys. Rev. Lett. **58**, 49 (1987).
[49]A. Sher, M. A. Berding, S. Krishnamurthy, M. van Schilfgaarde, A.-B. Chen, and W. Chen, Mater. Res. Soc. Symp. Proc. (to be published).
[50]N. E. Christensen and O. B. Christensen, Phys. Rev. B **33**, 4739 (1986).
[51]N. A. Cade and P. M. Lee, Solid State Commun. **56**, 637 (1985).
[52]A. V. Savitskii, M. V. Kurik, and K. D. Tovstyuk, Opt. Spectrosc. **19**, 59 (1964).
[53]D. G. Thomas, J. Appl. Phys. **32**, 2298 (1961).
[54]Y. Guldner, C. Rigaux, M. Grynberg, and A. Mycielski, Phys. Rev. B **8**, 3875 (1973).
[55]M. Cardona and D. L. Greenaway, Phys. Rev. **131**, 98 (1963).
[56]D. T. Marple and H. Ehrenreich, Phys. Rev. Lett. **8**, 87 (1962).
[57](a) A. Moritani, K. Taniguchi, C. Hamaguchi, and J. Nakai, J. Phys. Soc. Jpn. **34**, 79 (1973); (b) P. M. Amirthara, F. H. Pollak, and J. K. Furdyna, Solid State Commun. **39**, 35 (1981).
[58]M. Cardona and G. Harbeke, Phys. Rev. Lett. **8**, 90 (1962).
[59]M. Cardona, in *Modulation Spectroscopy, Solid State Physics Suppl. 11*, edited by F. Seitz, D. Turnbull, and H. Ehrenreich (Academic, New York, 1969), pp. 65–73; see also K. S. Song, J. Phys. (Paris) **28**, 195, Suppl. C3–C4 (1967).
[60]J. C. Phillips, in *Bonds and Bands in Semiconductors* (Academic, New York, 1973), pp. 178–187.
[61]S. H. Groves, R. N. Brown, and C. R. Pidgeon, Phys. Rev. **161**, 779 (1967).
[62]G. A. Antcliffe, Phys. Rev. B **2**, 345 (1970).
[63]H. Kahlert and G. Bauer, Phys. Rev. Lett. **30**, 1211 (1973).
[64]B. D. McCombe, R. J. Wagner, and G. A. Prinz, Phys. Rev. Lett. **25**, 87 (1970).
[65]M. A. Kinch and D. D. Buss, J. Phys. Chem. Solids **32**, 461 (1971).
[66]C. Verie and E. Decamps, Phys. Status Solidi **9**, 797 (1965).
[67]D. J. Olego, J. P. Faurie, and P. M. Raccah, Phys. Rev. Lett. **55**, 328 (1985).
[68]C. Verie, F. Raymond, J. Besson, and T. N. Duy, J. Cryst. Growth **59**, 342 (1982).
[69]W. A. Harrison, J. Vac. Sci. Technol. **14**, 1016 (1977).
[70]S.-H. Wei and A. Zunger, Phys. Rev. Lett. **59**, 144 (1987).
[71]S.-H. Wei and A. Zunger, J. Vac. Sci. Technol. B **5**, 1239 (1987). In this paper we have made mistakes in calculating apparent chemical shift (ACS) and true chemical shift (TCS) for AlAs/GaAs pairs. In Table I the ACS in the column of AlAs/GaAs should read 0.89, 0.85, 0.86, 0.84, 0.84, and 0.83, instead of 0.836, 0.809, 0.812, 0.838, 0.840, and 0.834. The average value should be $0.86 \pm 0.03$, instead of $0.825 \pm 0.016$. In Table II the TCS in the column of AlAs/GaAs should read 0.45, 0.45, and 0.46, instead of 0.423, 0.408, and 0.411. The average is 0.45 instead of 0.416. The results of $\Delta E_{\mathrm{VBM}}(\mathrm{AlAs/GaAs}) = 0.41 \pm 0.03$ eV are correct. Results obtained from our recent calculation of an $(\mathrm{AlAs})_2(\mathrm{GaAs})_2$ superlattice find $\Delta E_{\mathrm{VBM}}(\mathrm{AlAs/GaAs})$ to be $\sim 0.1$ eV larger than the results for $(\mathrm{AlAs})_1(\mathrm{GaAs})_1$. The dependence of the calculated $\Delta E_{\mathrm{VBM}}$ on superlattice thickness is expected to be smaller for II–VI's because of their smaller charge transfer effects.

[72]S. P. Kowalczyk, J. T. Cheung, E. A. Kraut, and R. W. Grant, Phys. Rev. Lett. **56**, 1605 (1986).
[73]T. M. Duc, C. Hsu, and J. P. Faurie, Phys. Rev. Lett. **58**, 1127 (1987).
[74]M. Pessa and O. Jylhä, Appl. Phys. Lett. **45**, 646 (1984).
[75]The tight-binding results are obtained using our semirelativistic local density orbital energies, see Ref. 70.
[76]A. Sher, A.-B. Chen, and M. van Schilfgaarde, J. Vac. Sci. Technol. A **4**, 1965 (1986).
[77]K. Beshah, D. Zamir, P. Becla, P. A. Wolff, and R. G. Griffin, Phys. Rev. B **36**, 6420 (1987).
[78]D. B. Zax, S. Vega, N. Yellin, and D. Zamir, Chem. Phys. Lett. **130**, 105 (1987).
[79]D. Zamir, K. Beshah, P. Becla, P. A. Wolff, R. G. Griffin, D. Zax, S. Vega, and N. Yellin, J. Vac. Sci. Technol. A **6**, 2612 (1988) (these proceedings).
[80](a) V. A. Terekov, V. M. Kashkarov, Yu. A. Teterin, I. M. Rarenko, and E. P. Domashevskaya, Sov. Phys. Semicond. **20**, 1038 (1986); (b) R. Sporken, S. Sivananthan, J. Reno, and J. P. Faurie (unpublished).
[81]J. L. Martins and A. Zunger, Phys. Rev. B **30**, 6217 (1984).
[82]A. Balzarotti, M. T. Czyzyk, A. Kisiel, P. Letardi, N. Motta, M. Podgorhy, and M. Zimnal-Starnawska, Festkoerperprobleme **25**, 689 (1985).
[83]J. Bernard and A. Zunger, Phys. Rev. B **36**, 3199 (1987).
[84]D. M. Wood, S.-H.Wei, and A. Zunger, Phys. Rev. B **37**,1342 (1988).
[85]J. P. Perdew and A. Zunger, Phys. Rev. B **23**, 5048 (1981).
[86]J. C. Brice, in *Properties of Mercury Cadmium Telluride*, Data Review Series (Inspec., London, 1987), p. 103.
[87]B. Toulouse, R. Granger, S. Roll, and R. Triboulet, J. Phys. (Paris) **48**, 247 (1987).
[88]V. G. Sredin, Sov. Phys. Semicond. **12**, 1084 (1978); V. A. Tyagai, O. V. Snitko, V. N. Bondarenko, N. I. Vitrikhovskii, V. B. Popov, and A. N. Krasiko, Sov. Phys. Solid State **16**, 885 (1974); K. Saito, A. Ebina, and T. Takahashi, Solid State Commun. **11**, 841 (1972).
[89]M. A. Berding, A.-B. Chen, and A. Sher (unpublished).